NJC

ROYAL SOCIETY OF CHEMISTRY

PAPER

View Article Online
View Journal

Cite this: DOI: 10.1039/d1nj02134f

Phenanthroimidazole derivatives showing mild intramolecular charge transfer and high quantum yields and their applications in OLEDs†‡

Swati J. N. Dixit,[a] Chandan Gupta,[b] Tanveer Habib Tadavi,[a] K. R. S. Chandrakumar,[c] Sangita Bose[b] and Neeraj Agarwal *[a]

Received 1st May 2021,
Accepted 27th July 2021

DOI: 10.1039/d1nj02134f

rsc.li/njc

Phenanthroimidzole (Phen-I) has attracted the attention of researchers for applications in materials science including organic electronics and biological applications. Herein, we designed small Phen-I derivatives showing mild bipolar characters and strong emissions in the blue region and discussed their applications in OLEDs. Designing of materials is based on the presence of electron-deficient nitrogen (sp^2) (acting as the mild electron-withdrawing core) and the availability of other nitrogen (N1) and carbon (C2) atoms for substitution at the imidazole ring. Earlier studies on the structural properties of Phen-I and our theoretical studies show that substitution at N1 is orthogonal to the plane of the imidazole ring, thus limiting the effect of extended conjugation. The aryl groups at the C2-carbon of the imidazole moiety caused considerable alteration in the electronic properties which is evident from the absorption and emission spectra. Absorption and emission in different solvents show slight alterations in the peak maxima suggesting mild intramolecular charge transfer in these molecules. These materials were also studied in thin films when doped in blends with polyvinylcarbazole (PVK). Furthermore, one of these Phen-I derivatives is used for OLED applications. A high luminance of $\sim 2.5 \times 10^4$ Cd m^{-2} at a current density of 35 mA cm^{-2} was found for Phen-I based OLEDs. This gave a high current efficiency of $\sim$ 60 Cd A^{-1} (@ 15 V) and an external quantum efficiency of $\sim$3.2%.

Introduction

The design and development of organic materials showing narrow luminescence in the red, green and blue regions has been an active research area for about three decades.[1–3] Their applications in organic electronics including organic light-emitting diodes (OLEDs) for lighting, display technologies, amplified spontaneous emissions, in organic solid-state lasers, *etc.* are the driving force for extensive research on suitable and efficient luminophores.[4] Compared to green and red emitters, the development of blue emitters with high color purity and stability for solid-state device applications is considered to be difficult.[5] Several rigid conjugated systems, starburst systems composed of various emitters, including fused aryl/heteroaryl derivatives of pyrene,[6] fluorene,[7] carbazole,[8] anthracene,[9] and phenanthroimidazole[10] (Phen-I), and donor–acceptor (D–A) systems[11] have been reported as emitters of different colors. In the design and development of blue emitters, challenges arise from (i) broad emissions due to the extended conjugation on the substitution of aromatic groups resulting in mixing of colors, (ii) poor oxidative stability of blue emitters causing keto defects, and (iii) strong aggregation in thin films which leads to band broadening and/or quenching of fluorescence.[12,13] A mild charge transfer character is advantageous for solid-state devices as it brings a slight bipolar nature which helps in the balanced transport of charge carriers to the respective electrodes.[14]

Imidazole and phenanthroimidazole have been known for few decades and their derivatives have been reported for various studies and applications.[15] Phen-I based materials are luminescent materials which show high fluorescence quantum yield, thermal stability, and good thin film forming properties. Owing to these properties, Phen-I attracts the attention of researchers for applications in materials science. Phen-I has been used in solid-state devices such as emitters, electron

[a] *School of Chemical Sciences, UM-DAE, Centre for Excellence in Basic Sciences, University of Mumbai, Kalina campus, Santacruz (E), Mumbai 400098, India. E-mail: na@cbs.ac.in*
[b] *School of Physical Sciences, UM-DAE, Centre for Excellence in Basic Sciences, University of Mumbai, Kalina Campus, Santacruz (E), Mumbai 400098, India*
[c] *Theoretical Chemistry Division, Bhabha Atomic Research Center, Trombay, Mumbai, India*

† This research work is part of PhD thesis of Ms Swati Dixit to be submitted to the University of Mumbai.

‡ Electronic supplementary information (ESI) available: NMR, absorption, emission, and MALDI-TOF spectra, and cyclic voltammograms for **1–7**. See DOI: 10.1039/d1nj02134f

transporters, hole blockers, sensitizers in solar cells, sensors, piezomaterials, *etc.*[16] Materials consisting of phenanthrene and imidazole moieties, *e.g.*, BCP, 4,7-diphenyl-1,10-phenanthroline (BPhen), and 2,2′,2″-(1,3,5-benzenetriyl)-tris-(1-phenyl-1*H*-benzimidazole) (TPBi), are being used as electron-transport facilitating materials in OLED devices.[17] Designing of Phen-I derivatives is based on (i) the availability of one sp^2 hybridized nitrogen which makes it moderately electron deficient thus acting as the mild electron-withdrawing core and (ii) the other nitrogen is in tetrahedral geometry, therefore, substitution on it is expected to be out of the Phen-I core. Therefore, substitution at tetrahedral N will have a limited effect of extended conjugation. Considering these two important aspects, we synthesized Phen-I derivatives aiming for strong blue emission and mild ICT properties. We introduced aryl substituents of varying electron densities and conjugation lengths at imidazole (C and N) and studied their detailed photophysical and electroluminescence properties.

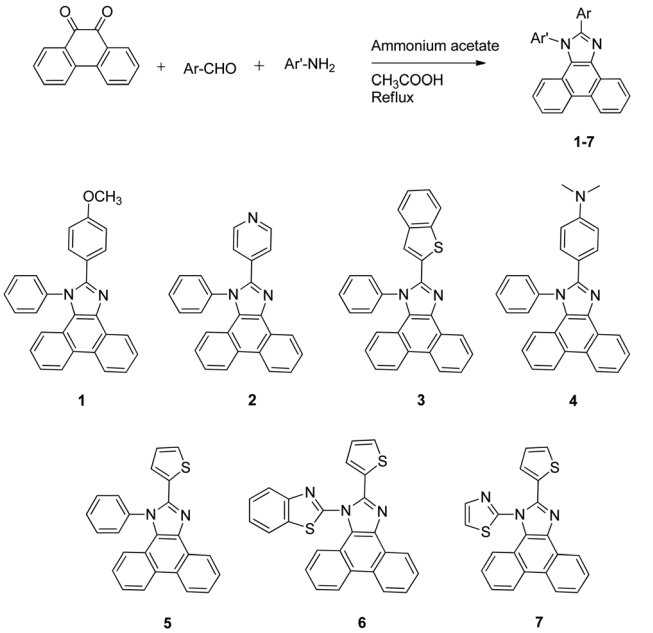

Scheme 1 Synthesis of phenanthroimidazole derivatives (**1–7**)

Results and discussion

Synthesis

A synthetic procedure is adopted for Phen-I derivatives using single-step condensation reactions between 9,10-phenanthrenequinone, aromatic amine and aromatic aldehyde in the presence of glacial acetic acid and ammonium acetate.[18] In this reaction, an aryl-substituted imidazole ring is formed. The aryl substituent at the nitrogen and carbon (sp^2) of the imidazole ring is obtained from the aromatic amine and aromatic aldehyde, respectively, used in this reaction. We believe that aryl substitution at the nitrogen will not be in the plane of the core phenanthroimidazole and will be somewhat orthogonal to the plane (see molecular geometry obtained from DFT calculations). Thus, we expect a minimum effect of this aryl group on π-conjugation. However, the aryl substituent on the carbon is expected to be in a similar plane to that of the phenanthroimidazole core and hence should affect the electronic properties considerably. Taking this into account, we have designed and synthesized phenanthroimidazole derivatives **1–7** as shown in Scheme 1. In **1–5**, N1 substitution is kept as phenyl while the substituent at the C2-carbon of the imidazole moiety is varied as anisyl (**1**), pyridyl (**2**), benzothienyl (**3**), *p*-*N*,*N*′-dimethylphenyl (**4**) and thienyl (**5**). In **5–7**, thiophene is at the C2-carbon position while phenyl (**5**), benzothiazole (**6**) and thiazole (**7**) are placed at the N1 position of imidazole. These compounds were characterized by ^{1}H-NMR, ^{13}C-NMR, and mass spectrometry. Analysis of the ^{1}H and ^{13}C NMR spectra suggests the proposed structures of the synthesized Phen-I derivatives. The MALDI-TOF spectra were consistent with the corresponding molecular weight of **1–7**, and the associated NMR and mass spectra are given in the ESI.‡

Photophysical studies

Absorption. The photophysical properties of Phen-I derivatives **1–7** were studied in solution and thin films using absorption and emission spectroscopies. Absorption and emission spectra of **1–7** recorded in dichloromethane are shown in Fig. 1(a) and (b), respectively, and a few photophysical observations obtained for **1–7** are summarized in Table 1. The absorption spectra of **1–7** revealed that these compounds have more or less similar absorption properties and show two or three absorption peaks between 320 and 380 nm. These peaks are assigned to the π–π* transitions of Phen-I and aromatic groups.[14] A slight shift towards the lower energy region in the absorption spectra is attributed to the delocalized π–π* transition extending from the phenanthroimidazole core to the substituted aryl groups. The extinction coefficients of **3**, **6** and **7** are observed to be higher than those of other derivatives. It has been reported earlier that an extinction coefficient related to π–π* transitions increases with the increase of conjugation length.[19] Absorption peaks are somewhat broad which could be due to the intramolecular charge transfer from the electron-donating moiety to the electron-accepting core of Phen-I. Different aryl groups (part of aryl aldehyde during the synthesis) at the C2-carbon of the imidazole moiety caused considerable alteration in the electronic properties which is evident from the absorption spectra of **1–5**. Interestingly, marginal shifts in the absorption peaks were observed when the aryl groups at N1 were varied (in the case of **5–7**) (see the elaborated figure in the ESI‡). Thus, we can infer that the electronic properties altered as expected and proposed in our design of Phen-I derivatives.

Emission. The emission spectra of **1–7** (Fig. 1(b)) show maxima between ∼390 and 411 nm. Vibronic features were observed in low polarity solvents which vanish in highly polar solvents. A shoulder in the lower energy region was observed at 425–440 nm in compounds **3–7**. Compounds **3** and **4** showed the most red-shifted emission which is assigned to the extended π-conjugation in **3** and the effect of strong

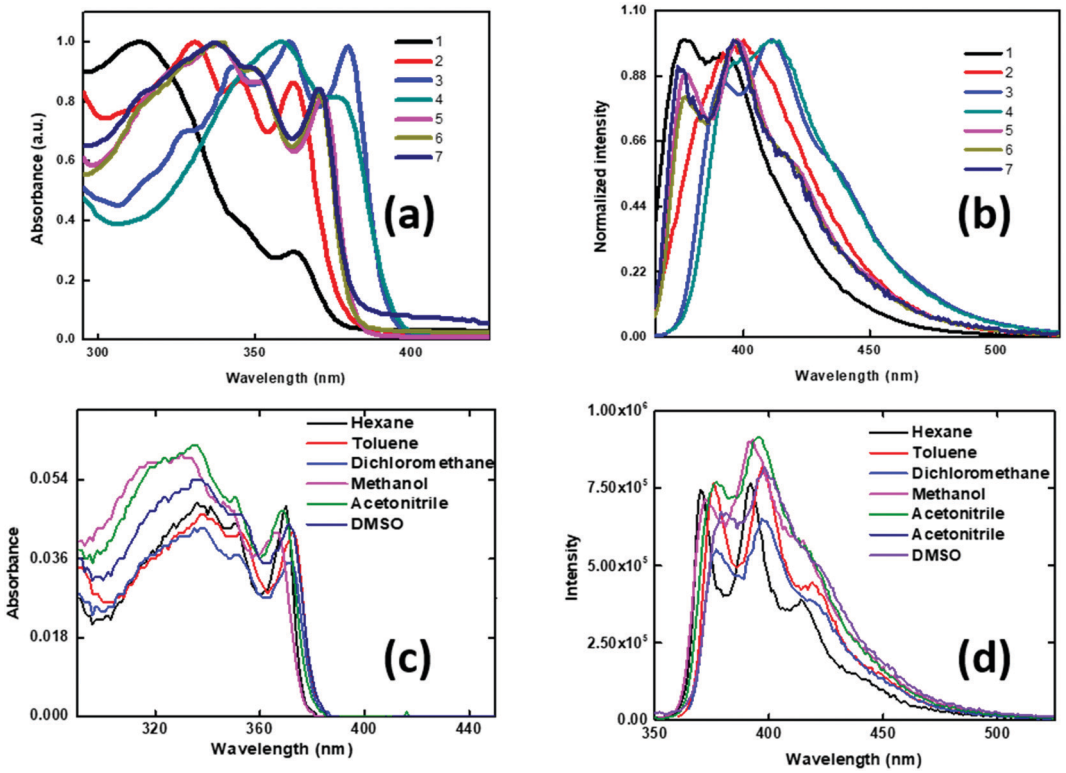

Fig. 1 (a) Absorption and (b) emission spectra of **1–7** in dichloromethane; (c) absorption and (d) emission spectra of **5** in different solvents.

Table 1 Photophysical properties of **1–7** in dichloromethane and thin films

	In dichloromethane					In thin films	
Comp.	λ_{abs} in nm (log ε)	λ_{em} (nm)	Stokes shift (cm^{-1})	ϕ^a (%)	τ (ns)	λ_{abs} (nm)	λ_{em} (nm)
1	315 (4.98), 363 (4.48)	377, 392	2030	45	5.11	315, 367	403
2	331 (4.85), 345 (3.82), 362 (4.78)	396	2370	73	2.11	339, 368	465
3	343 (6.17), 361 (6.20), 379 (6.19)	391, 411	2050	64	1.18	349, 368, 388	461
4	359 (5.39), 379 (4.29)	396, 411	2051	90	1.58	339, 372	451
5	338 (5.34), 352 (5.27), 371 (5.25)	376, 397	1770	55	1.90	344, 377	430
6	338 (6.34), 370 (6.25)	376, 396	1771	54	1.90	344. 378	407
7	337 (6.03), 370 (5.95)	375, 396	1774	50	1.96	348, 376	406, 436

[a] W.r.t. 9,10-diphenylanthracene in cyclohexane (ϕ = 90%).

electron-donating group in **4**. Compounds **5–7** showed almost identical emission spectra as observed in the absorption spectra too. This observation further emphasizes that N1 substitution causes a minimal effect on the electronic properties. To compare the emission properties of **1–7**, phenanthroimidazole was taken as standard which shows emission at 375 nm in dichloromethane.[14b] A bathochromic shift of ~20 nm for **1**, **2**, **5–7** and ~35 nm for **3**, **4** was observed. This red-shift is much smaller as compared to other literature-reported donor–acceptor systems of phenanthroimidazole core which suggests that, in our system, donor and acceptor moieties are of mild nature.[20]

To understand the donor–acceptor nature of **1–7**, we studied the absorption and emission properties in different solvents of varying polarity (Fig. 1c, d and ESI‡). It is found that absorption maxima do not change or change very slightly with a varying solvent polarity which indicates the non-polar nature of the ground state. Broadening of spectra with loss of vibronic features in polar solvents was observed. The interaction of the excited state with polar solvents may be the reason behind the loss of vibronic features in high polarity solvents. A marginal, though considerable, red-shift is observed in high polarity solvents which indicates the polar nature of the excited state. Compound **1** showed emission maxima at 386 nm in hexane while 391 nm in DMSO, a shift of 5 nm. Compound **2** showed peaks at 381 and 414 nm (a shift of 33 nm), **3** showed peaks at 403 and 414 nm (a shift of 11 nm), and **4** showed peaks at 396 and 429 nm (a shift of 33 nm). Compounds **5–7** showed a negligible red-shift in emission in hexane and DMSO. Emission spectra arising from locally excited (LE) S_0–S_1 do not show

Table 2 Quantum yield, ϕ (%), fluorescence lifetimes, and τ (ns) of **1–7** in different solvents

Compound	**1**		**2**		**3**		**4**		**5**		**6**		**7**	
Solvent	ϕ	τ	ϕ	τ	ϕ	τ	ϕ	τ	ϕ	τ	ϕ	τ	ϕ	τ
Hexane	33	4.21	71	2.43	55	1.00	98	1.63	48	1.60	51	1.59	48	1.83
Toluene	41	4.99	73	2.03	68	1.06	86	1.37	58	1.62	65	1.87	62	1.96
DCM	38	5.11	72	2.11	64	1.18	90	1.58	53	1.90	54	1.90	50	1.83
Methanol	45	6.05	83	1.07	68	1.22	94	1.59	53	1.91	66	2.82	61	2.79
Acetonitrile	40	5.76	84	2.23	72	1.26	87	2.08	53	2.52	56	3.58	56	3.51
DMSO	53	7.59	89	2.37	73	1.30	93	2.02	57	2.29	68	3.95	63	—

dependency on solvent polarity whereas emission arising due to charge transfer (CT) states alters with the polarity of the solvent medium.[21] The solvatochromic effect is considered to be the measure of intramolecular charge transfer (ICT), where more shift indicates stronger ICT. Here, our studied compounds **5–7** showed smaller bathochromic shifts than compounds **1–4** which resulted in mild ICT in **5–7**. Nevertheless, the solvatochromic shifts in **1–4** are considerably smaller than many other donor–acceptor systems known in the literature.

The fluorescence quantum yield of these compounds was calculated with respect to 9,10-diphenylanthracene (ϕ = 90% in cyclohexane).[22] Compounds **1–7** showed high to very high quantum efficiency. Interestingly, these compounds showed high quantum yield (~50–98%) in polar as well as non-polar solvents (Table 2). To understand the excited state properties, the fluorescence decay profiles of compounds **1–7** were recorded using the TCSPC method and their decay traces are shown in the ESI.‡ The lifetime decay of **1–7** is found to be mono-exponential in solution. Compounds **2–7** showed fluorescence decay time of <2 ns in dichloromethane and, for **1**, it is ~5 ns. The fluorescence lifetimes of **1–7** in different solvents are summarized in Table 2. It is also observed that lifetimes increase slightly as we increase the polarity of solvents (Table 2). The fluorescence decay profiles of **5** recorded in different solvents are shown in Fig. 2. From the photophysical studies, we conclude that these chromophores have mild ICT and high fluorescence quantum yields.

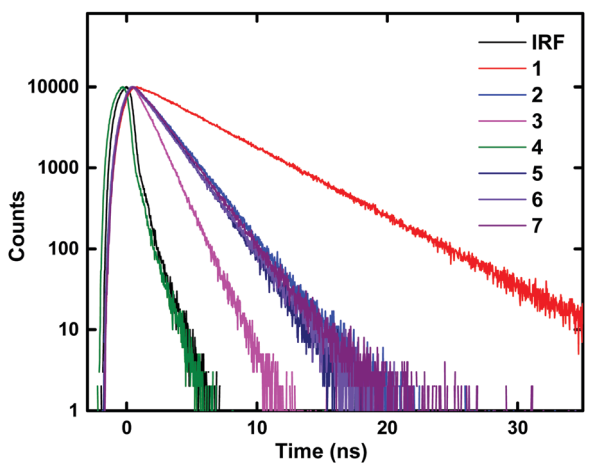

Fig. 2 Fluorescence decay profiles of **1–7** in DCM.

Emission studies in thin films. Fluorescent materials sometimes exhibit different properties in thin films than in solution. They show interesting properties such as energy transfer, triplet state population, exciplex formation, quenching of emission, *etc.* when doped in host materials consisting of small molecules or polymers.[23] Thus, it can be envisaged that emission can be controlled by having suitable host materials. The emission intensity and color can be tuned to some extent by the varying amount of interactions between the host and guest molecules. Many times small organic materials show red-shifted emission in thin films and these spectral shifts are believed to be due to the aggregation behaviour. The emission spectra of **1–7** in spin-coated thin films are shown in the ESI.‡ A slight red-shift was observed in these compounds which is attributed to the varying amounts of aggregation in thin films. We further studied the effect of host molecules on the emission properties of **1–7**. The interaction of **1–7** in the polymeric host matrix of polyvinyl carbazole (PVK) was studied in thin films of their blends. Blends of 1 : 2 and 1 : 4 (w/w) were prepared and thin films were spin-coated on quartz plates. Fig. 3 shows the emission of neat **2**, **3** and **5** and their blends with PVK. Neat PVK shows emission at ~406 nm while **2** shows emission at 466 nm, **3** at 462 nm and **5** at 466 nm (Fig. 3) in thin films. The thin films of PVK and **2**, **3** and **5** (blends in 1 : 2 and 1 : 4 ratios) show new emission peak maxima at 398 nm for **2**, at 415 and 394 nm for **3**, and at 403 and 381 nm for **5**. These new peaks in blends do not match with the thin film emission of the individual material. Interestingly, new emission features in PVK blends of **2**, **3** and **5** match the solution spectra closely. The resemblance with solution spectra suggests the suppression of the intermolecular interaction of molecules in thin films. With the aggregation behaviour of the PVK blends of these Phen-I derivatives, red-shifting of emission could be minimized.

Electrochemical studies

The redox behaviour of Phen-I derivatives **1–7** was studied using cyclic voltammetry in an acetonitrile/DCM mixture. Tetrabutylammonium hexafluorophosphate (0.1M) was used as a supporting electrolyte. Ferrocene was used as an internal standard and the oxidation potential of Fc/Fc^{+} is considered as a reference potential. Two irreversible oxidation waves were observed for **1–7**. The first oxidation potentials were found in the range of 0.96–1.47 V for **1–7**. The oxidation potential for **4** was the lowest among them which suggests that it could be oxidized easily as compared to others. Compound **2** having the

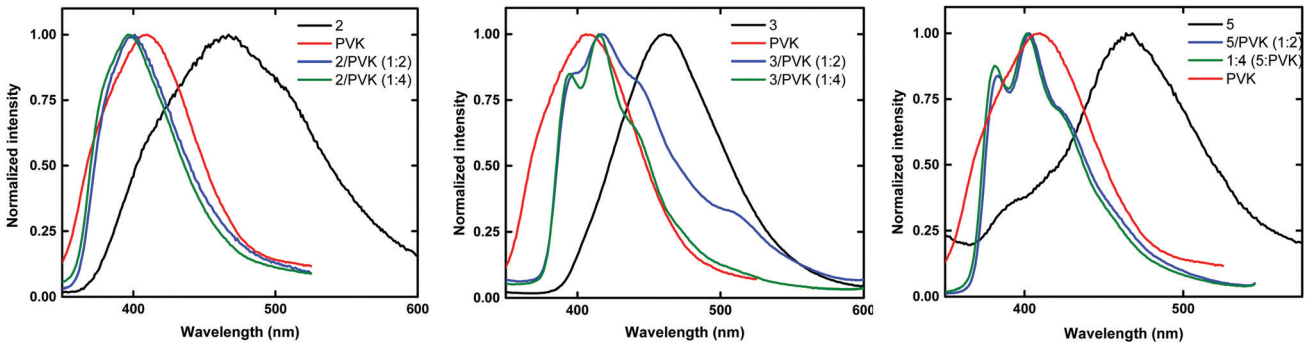

Fig. 3 Emission studies in thin films for **2**, **3** and **5** and their PVK blends.

electron-accepting pyridine group was difficult to oxidize and showed higher oxidation potential. The cyclic voltammograms of **1–7** are shown in the ESI.‡ The highest occupied molecular orbital (HOMO) and the lowest unoccupied molecular orbital (LUMO) energy levels for **1–7** were estimated using the first oxidation potentials and optical band gaps.[24] The HOMO and LUMO energy levels for **1–7** are summarized in Table 3. It is worth noting here that the E_{HOMO} of these compounds varies with the aryl group. For example, the E_{HOMO} of **2** (having pyridine) is −6.09 eV and that of **4** (having *N*,*N*-dimethylphenyl) is −5.57 eV. We could not observe the reduction peaks for these compounds under our experimental conditions. The optical band gap of **1–7** was measured from the intersection of excitation and emission spectra. E_{LUMO} was calculated using E_{HOMO} and optical band gaps. The E_{HOMO}, optical band gaps and E_{LUMO} are summarized in Table 3.

Theoretical studies

Quantum chemical calculations were performed on **3** and **5** to understand the effect of the phenyl group on the Phen-I derivatives and the origin of the photophysical properties. The geometry optimization and time-dependent DFT (TDDFT) based calculations for the evaluation of electronic excitation spectra were performed using Becke's three-parameter exchange functional and the Lee–Yang–Parr correlation functional (B3LYP exchange–correlation functional).[25,26] The geometry of **3** and **5**, having the phenanthroimidazole unit with one phenyl group situated at the N1 of the imidazole ring, is initially optimized and the corresponding structures are shown in Fig. 4. It can be seen that the phenyl group is perpendicular to the phenanthroimidazole ring and the planar angle difference is found to be 96 degrees. Similarly, the calculated HOMO–LUMO gap of molecules **3** and **5** is 3.56 and 3.71 eV, which is found to be in good agreement with the experimental values of 3.21 and 3.30 eV, respectively, obtained from the optical band gap measurement (Table 3). Although the optical band gap is found to be very close to the computed values, the HOMO and LUMO values are observed to be slightly underestimated.

The frontier molecular orbital density plots (HOMO−1, HOMO, LUMO and LUMO+1) are shown in Fig. 5, indicating that the HOMO is exclusively contributed by the phenanthroimidazole core units whereas the LUMO is mostly contributed by the thienyl group. Also, it can be seen from Fig. 5 that the HOMO−1 is mostly localized on the phenanthroimidazole as well as thienyl groups from where the electronic transitions are assumed to take place, *i.e.*, HOMO−1 to LUMO as well as LUMO+1 instead of HOMO–LUMO.

The absorption spectra calculated by the TD-DFT method for **3** and **5** are shown in Fig. 6. The calculated oscillator strengths and the maximum wavelengths (λ) along with their orbital assignments for compounds **3** and **5** are presented in Table 4. For **3**, at the equilibrium geometry, the spectrum shows one major peak at 370.3 and other small peaks at 352.3 and 286.7 nm. Similarly, for **5**, three dominant peaks are observed at 360.9, 348.1 and 273.9 nm. By inspecting Table 4, it can be seen that for both **3** and **5**, the first two peaks are the result of the electronic transitions from the HOMO to LUMO as well as

Table 3 Electrochemical data of **1–7** in acetonitrile

Compound	E_{ox}[a] (V)	HOMO[b] (eV)	LUMO[c] (eV)	Optical band gap[d] (eV)
1	0.76, 1.11	−5.86	−2.43	3.43
2	0.98, 1.20	−6.09	−2.75	3.34
3	0.73, 0.96	−5.83	−2.62	3.21
4	0.47, 0.84	−5.57	−2.37	3.20
5	0.69	−5.79	−2.49	3.30
6	0.59, 0.95	−5.69	−2.38	3.31
7	0.59, 1.08	−5.69	−2.35	3.34

[a] W.r.t. Fc/Fc^+. [b] $E_{HOMO} = -(E_{[ox\ vs.\ Fc/Fc^+]} + 5.1)$ eV. [c] $E_{LUMO} = E_{HOMO}$ + optical band gap eV. [d] Obtained from the intersection of excitation and emission spectra in thin films.

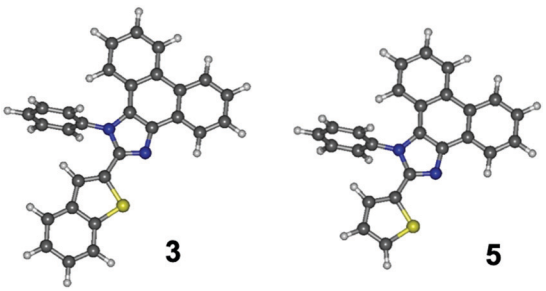

Fig. 4 Optimized geometry of compounds **3** and **5**.

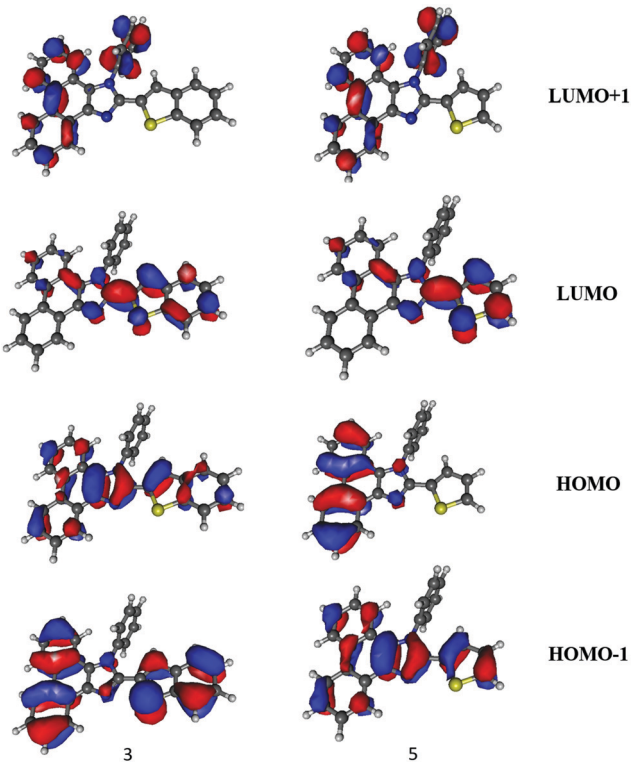

Fig. 5 The frontier orbitals (HOMO−1, HOMO, LUMO and LUMO+1) of **3** and **5**.

from the HOMO to LUMO+1. However, the third peak originates from the excitation of HOMO−2/HOMO−1 to LUMO/LUMO+1. A general analysis of these frontier orbitals indicates that the electron density is transferred predominantly from the phenanthroimidazole-based aromatic groups to the thienyl or benzothienyl rings. Interestingly, it can also be observed that the low intensity peak located at 352.3 nm in **3** and at 273.9 nm in **5** is mostly associated with the HOMO to LUMO+1 transition, which shows the dominant charge transfer from the phenanthroimidazole-based aromatic groups to the aryl groups. It may be noted that such transition probabilities are less. This is illustrated in terms of isodensity molecular orbital plots as presented in Fig. 5.

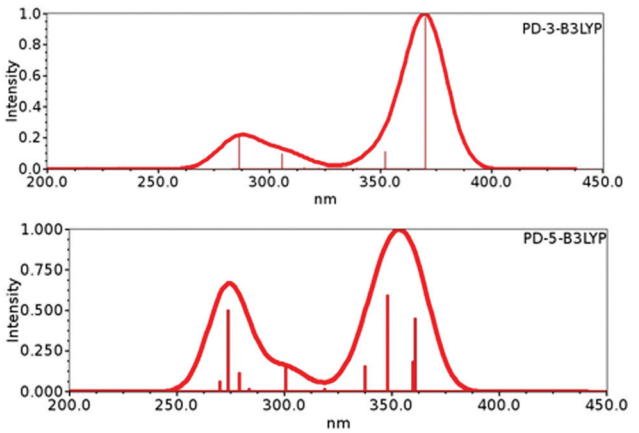

Fig. 6 Simulated absorption spectra of **3** (above) and **5** (below).

Table 4 Dominant optical transition characters for the lowest excitation states of **3** and **5**, calculated by the TDDFT-based B3LYP method

Compound	Oscillator strength	$^{abs}\lambda_{max}$ (nm)	Orbital transitions
3	0.950	370.3	HOMO → LUMO
	0.112	352.3	HOMO → LUMO+1
	0.201	286.7	HOMO−2 → LUMO
5	0.242	360.9	HOMO → LUMO
	0.361	348.1	HOMO → LUMO and HOMO → LUMO+1
	0.269	273.9	HOMO−1 → LUMO and HOMO−1 → LUMO+1

Organic light-emitting devices

A suitable amount of intramolecular charge transfer in fluorescent materials is considered beneficial for high efficiency OLEDs. Materials with very small ICT are expected to show bipolar charge transport imparting balanced holes and electrons in the device. Compound **5** was used to study the electroluminescence properties and OLEDs were fabricated with the following device geometry: ITO/PEDOT:PSS (50 nm)/NPD (50 nm)/**5** (70 nm)/Bphen (25 nm)/LiF (2–5 nm)–Al (120 nm). *N*,*N*′-Di(1-naphthyl)-*N*,*N*′-diphenyl-(1,1′-biphenyl)-4,4′-diamine (NPD) was used as the hole transporting layer near the anode and 4,7-diphenyl-1,10-phenanthroline (Bphen) was used as the hole blocking layer (HBL) near the cathode. A few prominent results obtained for OLEDs are presented in Fig. 7. The electroluminescence (EL) spectra of OLEDs made of **5** showed a emission peak at ∼460 nm (see Fig. 7a) which shows a close resemblance with the photoluminescence of **5** in thin films. A weaker peak at ∼600 nm is also observed in the EL spectra which may be due to the electromer formation during the electrical excitation. We are currently investigating this in detail. The electroluminescence spectra of OLEDs at different voltages are being recorded now. The EL spectra at different voltages are found to be identical (see the ESI‡). The turn-on voltage, V_{ON}, was found to be 7 V (Fig. 7b). The devices showed a high luminance of $\sim 2.4 \times 10^4$ cd m^{-2} at a current density of 35 mA cm^{-2}. The current efficiency was also high (∼60 cd A^{-1}) and the external quantum efficiency was found to be ∼3.2% (Fig. 7c).

Conclusions

Phen-I derivatives showing mild bipolar characters and strong emissions in the blue region were synthesized and characterized. The aryl groups at the C2-carbon of the imidazole moiety caused considerable alteration while the aryl groups at N1 showed marginal shifts in the electronic properties as evident from the absorption and emission spectra. The photophysical properties in different solvents show evidence of mild intramolecular charge transfer. Also, a very high fluorescence quantum yield (>90%) is found for some of these compounds.

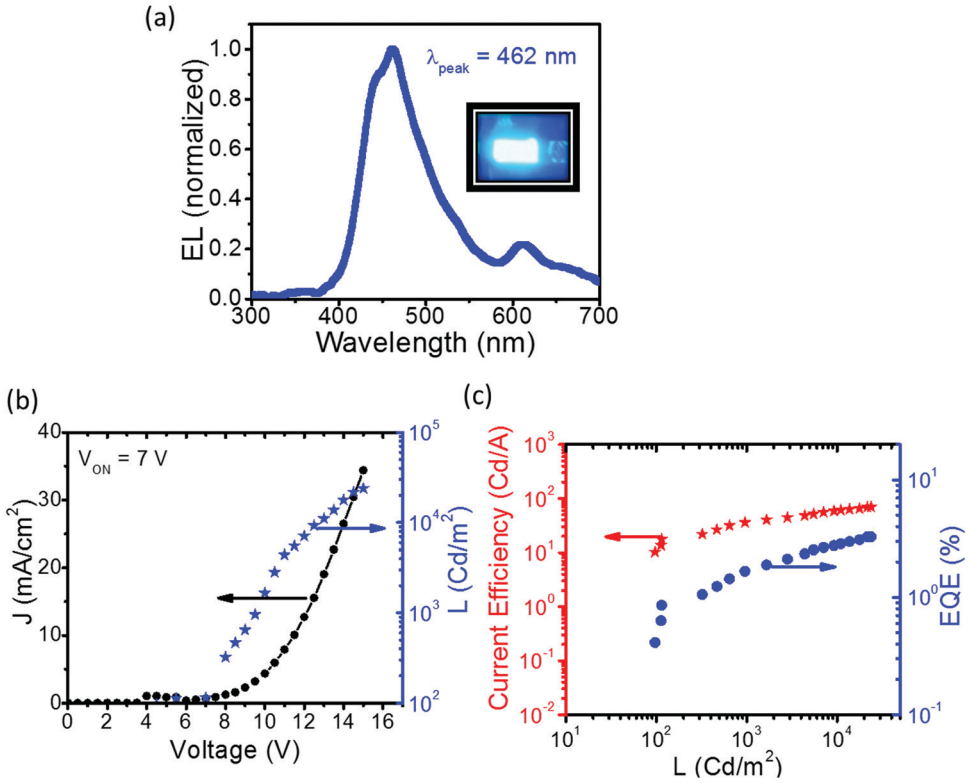

Fig. 7 Characteristics of OLEDs (ITO/PEDOT:PSS (50 nm)/NPD (50 nm)/**5** (70 nm)/Bphen (25 nm)/LiF (2–5 nm)–Al (120 nm)) fabricated with compound **5**.

The Phen-I derivatives were blended with PVK to study their interactions in the excited state. It was observed that the intermolecular interactions are suppressed in thin films in the presence of PVK and the emissions were found to be similar to those in solution. Furthermore, compound **5** is used in OLED applications. For OLEDs, the luminance is $\sim 2.5 \times 10^4$ cd m^{-2} at a current density of 35 mA cm^{-2}, with an external quantum efficiency of $\sim 3.2\%$. Our results convincingly show that these new Phen-I derivatives are highly emissive in the blue region and are promising materials for efficient OLED applications.

Experimental

Methods

Chemicals were purchased from SD Fine Chemicals, Sigma Aldrich, *etc.* and were used as received. Organic solvents of analytical and spectroscopic grades were used. ^{1}H and ^{13}C NMR were recorded using a Varian 600 or 800 MHz spectrometer. Residual chloroform in $CDCl_3$ was used as an internal reference. Mass spectra were recorded using a Bruker MALDI-TOF. Cyclic voltammetry was carried out on a CH Instruments (620D model) electrochemical workstation. For a CV three-electrode cell with glassy carbon as the working electrode, Ag/AgCl (non-aqueous) as the reference electrode and Pt wire as the counter electrode were used. Electrochemical studies were performed in a mixture of dichloromethane and acetonitrile with tetrabutylammonium hexafluorophosphate solution (0.1M) as a supporting electrolyte at a scan rate of 100 mV s^{-1}. Ferrocene was used as an internal standard reference. UV-vis spectra were obtained using a Shimadzu 1800 and the steady-state fluorescence spectra were recorded using a Horiba Fluoromax-4. A diode laser or a nano-LED-based time-correlated single-photon counting (TCSPC) spectrometer (Deltaflex, HORIBA) was used to obtain the time-resolved fluorescence measurements. The fluorescence transients were collected at the magic angle (54.7°) configuration. To obtain the instrument response function (IRF), the scattered excitation light from the suspended SiO_2 particles in water was monitored. All the theoretical calculations were performed using the ORCA electronic structure-based program. The RHF types of Kohn–Sham based density functional theory (DFT) methods have been employed. The geometry optimization and time-dependent DFT (TDDFT) based calculations for the evaluation of electronic excitation spectra have been performed using Becke's three-parameter exchange functional and the Lee–Yang–Parr correlation functional (B3LYP exchange–correlation functional). The grid-based DFT has been used which employs a typical grid quadrature for the computation of the integrals. Typically, the grid consists of 96 radial shells with 36 and 72 angular points during the SCF procedure. OLED devices were fabricated using thermal vacuum deposition which was performed at a base vacuum of 2×10^{-6} mbar. An ITO-coated substrate (15–25 Ω sq^{-1}, Sigma Aldrich) of dimensions 22 × 12 cm was initially etched to incorporate four independent active devices with the help of Zn powder and 10% HCl. Substrate cleaning was performed in

three simple steps. It was first cleaned with soap solution and rinsed with distilled water. Furthermore, it was sonicated with distilled water and propanol. The sonication time was 10 min for each step. This was followed by cleaning with trichloroethylene (TCE) vapors and drying using nitrogen. The cleaned substrates were kept under a UV lamp for 30 minutes. The layer of PEDOT:PSS was spin-coated onto the UV-treated substrates. Spin coating was performed at a speed of 6000 rpm for 45 seconds which gave a 50-nm-thick layer. The substrates were subsequently annealed at 160 °C for 30 minutes to give a hard, uniform layer of PEDOT:PSS. All the subsequent layers of NPD, compound **5**, BPhen, LiF and Al were thermally evaporated in vacuum. The first three layers were grown without breaking the vacuum to ensure clean interfaces with the active layer of compound **5**.

General method for the synthesis of 1–7

The compounds (**1–7**) were synthesized by refluxing the mixture of 9,10-phenanthrenequione (1 mmol), primary aromatic amine (1 mmol), ammonium acetate (1 mmol) and aromatic aldehyde (1 mmol) in glacial acetic acid for 24 h. The completion of the reaction was monitored by the TLC method. After completion, the reaction mixture was cooled to room temperature and water was added to precipitate the organic solids. The crude solid products were purified by silica gel column chromatography to obtain the pure **1–7** in 70–80% yield.

Characterization data

1. 9,10-Phenanthrenequione (0.2 g, 0.96 mmol), aniline (90 μL, 1.0 mmol), ammonium acetate (1.0 mmol) and anisaldehyde (1.0 mmol) in glacial acetic acid were used for synthesis as described in the general method. A pure white solid compound was obtained. Yield: (0.321 g, 80%). M.p.: >250 °C; ^{1}H-NMR (600 MHz, $CDCl_3$, δ ppm): 8.87 (d, 1 H, J = 7.8 Hz), 8.77 (d, 1 H, J = 8.4 Hz), 8.71 (d, 1 H, J = 8.4 Hz), 7.75–7.72 (t, 1 H, J = 7.8 Hz), 7.65–7.58 (m, 4 H), 7.51–7.48 (m, 5 H), 7.26–7.24 (m, 1 H), 7.17 (d, 1 H, J = 8.4 Hz), 6.82 (d, 2 H, J = 9 Hz), 3.79 (s, 3 H); ^{13}C NMR (200 MHz, $CDCl_3$): 160.10, 151.07, 139.00, 137.39, 130.89, 130.21, 129.78, 129.26, 129.19, 128.29, 128.03, 127.31, 126.31, 125.58, 124.78, 124.17, 123.19, 123.17, 123.10, 122.83, 120.84, 113.76, 55.31; MALDI-TOF: mass calcd for $C_{18}H_{20}N_2O$: 400.16, found: 400.37 $(M)^+$.

2. 9,10-Phenanthrenequione (0.2 g, 0.96 mmol), aniline (90 μL, 0.96 mmol), ammonium acetate (0.11 g, 0.96 mmol) and 4-pyridinealdehyde (0.10 g, 0.96 mmol) in glacial acetic acid were used for synthesis as described in the general method. A pure buff white solid compound was obtained. Yield: (0.274 g, 75%). M.p.: >250 °C; ^{1}H-NMR (600 MHz, $CDCl_3$, δ ppm): 8.86 (d, 1 H, J = 8.4 Hz), 8.77 (d, 1 H, J = 8.4 Hz), 8.71 (d, 1 H, J = 8.4 Hz), 8.53 (d, 2 H, J = 6 Hz), 7.77–7.74 (t, 1 H, J = 7.2 Hz), 7.73–7.70 (t, 1 H, J = 7.2, 7.2 Hz), 7.69–7.66 (m, 3 H), 7.55–7.52 (t, 3 H, J = 7.2, 7.2 Hz), 7.48 (d, 2 H, J = 6 Hz), 7.28 (d, 1 H, J = 7.8 Hz), 7.17 (d, 1 H, J = 7.8 Hz); ^{13}C NMR (200 MHz, $CDCl_3$):) 174.73, 149.31, 138.28, 138.22, 137.72, 130.61, 130.49, 129.75, 129.00, 128.82, 128.50, 127.54, 126.97, 126.50, 126.11, 125.57, 124.22, 123.21, 122.97, 122.73, 121.00; m.p.: >250 °C; HRMS: mass calcd for $C_{26}H_{17}N_3$: 372.1495, found m/z: 372.1495 $(M)^+$.

3. A mixture of 9,10-phenanthrenequione (0.20 g, 0.96 mmol), aniline (90 μL, 0.96 mmol), benzo[*b*]thiophene-2-carbaldehyde (0.16 g, 0.96 mmol) and ammonium acetate (0.11 g, 0.96 mmol) in acetic acid was refluxed for 24 h. A buff white solid compound was obtained. Yield: (0.306 g, 72%). M.p.: > 250 °C; ^{1}H-NMR (600 MHz, $CDCl_3$, δ ppm): 8.89 (d, 1 H, J = 8.4 Hz), 8.76 (d, 1 H, J = 8.4 Hz), 8.69 (d, 1 H, J = 8.4 Hz), 7.81–7.73 (m, 5 H), 7.67–7.65 (m, 3 H), 7.59 (d, 1 H, J = 7.8 Hz), 7.52–7.50 (t, 1 H, J = 7.2 Hz), 7.32–7.29 (m, 3 H), 7.16 (d, 1 H, J = 8.4 Hz), 6.96 (s, 1 H); ^{13}C NMR (200 MHz, $CDCl_3$): 145.65, 140.28, 139.79, 138.43, 137.84, 133.27, 130.78, 130.76, 129.52, 129.39, 128.79, 128.46, 127.39, 127.05, 126.49, 125.24, 124.53, 124.22, 124.53, 124.22, 123.49, 123.19, 123.05, 122.86, 122.03, 120.80; HRMS: mass calcd for $C_{29}H_{18}N_2S$: 427.1623, found: 427.1268 $(M)^+$.

4. A mixture of 9,10-phenanthrenequione (0.20 g, 0.96 mmol), aniline (90 μL, 0.96 mmol), 4-(dimethylamino)benzaldehyde (0.14 g, 0.96 mmol) and ammonium acetate (0.11 g, 0.96 mmol) in acetic acid was refluxed for 24 h. A pure yellowish white solid compound was obtained. Yield: (0.289 g, 70%). M.p.: >250 °C; ^{1}H-NMR (600 MHz, $CDCl_3$, δ ppm): 8.76–8.73 (t, 3 H, J = 9.00, 9.60 Hz), 8.63 (d, 1 H, J = 7.8 Hz), 8.33 (d, 1 H, J = 7.8 Hz), 8.24 (d, 3 H, J = 9 Hz), 7.75–7.64 (m, 6 H), 6.83 (d, 3 H, J = 8.4 Hz), 3.09 (s, 6 H); ^{13}C NMR (200 MHz, $CDCl_3$, δ ppm): 163.61, 152.17, 144.30, 135.84, 128.91, 128.76, 127.34, 127.25, 126.41, 125.91, 125.89, 123.83, 123.52, 123.10, 121.40, 120.77, 115.10, 111.82, 40.31; MALDI-TOF: mass calcd for $C_{29}H_{23}N_2S$: 413.19, found: 413.51 $(M)^+$.

5. 9,10-Phenanthrenequione (0.20 g, 0.96 mmol), aniline (90 μL, 0.96 mmol), ammonium acetate (0.11 g, 0.96 mmol) and thiophene-2-carbaldehyde (0.11 g, 0.96 mmol) in glacial acetic acid were used for synthesis as described in the general method. A pure white solid compound was obtained. Yield: (0.319 g, 85%). M.p.: > 250 °C; ^{1}H-NMR (600 MHz, $CDCl_3$, δ ppm): 8.86 (d, 1 H, J = 8.4 Hz), 8.79 (d, 1 H, J = 8.4 Hz), 8.69 (d, 1 H, J = 8.4 Hz), 7.76–7.61 (m, 4 H), 7.66–7.63 (t, 1 H, J = 7.8 Hz), 7.62 (d, 2 H, J = 7.8 Hz), 7.50–7.48 (t, 1 H, J = 7.8 Hz), 7.30 (d, 1 H, J = 5.4 Hz), 7.24–7.23 (d, 1 H, J = 7.8 Hz), 7.14 (d, 1 H, J = 8.4 Hz), 6.91–6.90 (t, 1 H, J = 4.2 Hz), 6.86 (d, 1 H, J = 3.6 Hz); ^{13}C NMR (200 MHz, $CDCl_3$): 145.99, 138.42, 137.54, 133.12, 130.59, 130.55, 129.35, 129.25, 128.32, 128.19, 127.51, 127.43, 127.27, 127.24, 127.02, 126.38, 125.71, 124.95, 124.13, 123.11, 122.93, 122.87, 120.60.; HRMS: mass calcd for $C_{25}H_{16}N_2S$: 377.1107, found: 377.1106 $(M)^+$.

6. 9,10-Phenanthrenequione (0.20 g, 0.96 mmol), benzo[*b*]thiazole-2-amine (145 g, 0.96 mmol), ammonium acetate (0.11 g, 0.96 mmol) and thiophene-2-carbaldehyde (0.11 g, 0.96 mmol) in glacial acetic acid were used for synthesis as described in the general method. A pure buff white solid compound was obtained. Yield: (0.35 g, 83%). M.p.: >250 °C; ^{1}H-NMR (600 MHz, $CDCl_3$, δ ppm): 8.73 (d, 3 H, J = 8.4 Hz), 7.69–7.66 (m, 4H), 7.64–7.61 (t, 4 H, J = 7.8 Hz), 7.43 (d, 2 H, J = 4.8 Hz), 7.16–7.15 (t, 2 H, J = 4.2 Hz).

7. 9,10-Phenanthrenequione (0.20 g, 0.96 mmol), thiazole-2-amine (0.1 g, 0.96 mmol), ammonium acetate (0.11 g,

0.96 mmol) and thiophene-2-carbaldehyde (0.11 g, 0.96 mmol) in glacial acetic acid were used for synthesis as described in the general method. A pure buff white solid compound was obtained. Yield: (0.303 g, 83%). ^{1}H-NMR (600 MHz, $CDCl_3$, δ ppm): 8.73 (d, 3 H, J = 8.4 Hz), 7.69–7.61 (m, 8 H), 7.43 (d, 1 H, J = 4.8 Hz), 7.15–7.14 (t, 1 H, J = 4.2 Hz); m.p.: > 250 °C; MALDI-TOF: mass calcd for $C_{22}H_{13}N_3S$: 383.50, found: 383.50 $(M)^+$.

Conflicts of interest

There are no conflicts to declare.

Acknowledgements

SD carried out the synthesis and photophysical studies and CG fabricated the OLEDs. SD thanks DST SERB for fellowship. We thank Mrs Mamata Joshi and Mrs Gitanjali Dhotre of Tata Institute of Fundamental Research, Mumbai, for NMR and MALDI-TOF, respectively. We are thankful to Indian Institute of Technology, Bombay, for providing the HRMS facility. NA and SB thank the Department of Science and Technology for partial financial support (EMR/2017/000805).

Notes and references

1 (*a*) A. Loudet and K. Burgess, *Chem. Rev.*, 2007, **107**, 4891–4932; (*b*) T. Boodts, E. Fron, J. Hofkens and W. Dehaen, *Coord. Chem. Rev.*, 2018, **371**, 1–10; (*c*) H. Liu, F. Liu and P. Lu, *J. Mater. Chem. C*, 2020, **8**, 5636–5661.

2 (*a*) C. W. Tang and S. A. Van Slyke, *Appl. Phys. Lett.*, 1987, **51**, 913–917; (*b*) R. Diana, B. Panunzi, F. Marrafino, S. Piotto and U. Caruso, *Polymers*, 2019, **11**, 1751; (*c*) A. K. Brett, Y.-L. Chang, Z.-H. Lu and T. P. Bender, *Electronics*, 2012, **13**, 1479–1485; (*d*) S. R. Forrest, *Nature*, 2004, **428**, 911–918; (*e*) P. K. Nayak, N. Agarwal, F. Ali, M. Patankar, N. Periasamy and K. L. Narasimhan, *J. Chem. Sci.*, 2010, **122**, 847–855.

3 (*a*) S. R. Forrest, M. A. Baldo, D. F. O'Brien, Y. You, A. Shoustikov, S. Sibley and M. E. Thompson, *Nature*, 1998, **395**, 151–154; (*b*) A. F. Rausch, H. H. H. Homeier and H. Yersin, *Top. Organomet. Chem.*, 2010, **29**, 193–235; (*c*) N. Agarwal and P. K. Nayak, *Tetrahedron Lett.*, 2008, **49**, 2710–2713; (*d*) J. Wang, Y. Wang, Y. Qin, R. Li, J. An, Y.-H. Chen, W.-Y. Lai, X.-W. Zhang and W. Huang, *J. Mater. Chem. C*, 2021, **9**, 8570–8578.

4 (*a*) H. Kaji, H. Suzuki, T. Fukushima, K. Shizu, K. Suzuki, S. Kubo, H. Oiwa, F. Suzuki, A. Wakamiya, Y. Murata and C. Adachi, *Nat. Commun.*, 2015, **6**, 8476–8483; (*b*) M. Y. Wong and E. Zysman-Colman, *Adv. Mater.*, 2017, **29**, 1605444; (*c*) S. M. King, M. Cass, M. Pintani, C. Coward, F. B. Dias, A. P. Monkman and M. Roberts, *J. Appl. Phys.*, 2011, **109**, 074502; (*d*) H. Uoyama, K. Goushi, K. Shizu, H. Nomura and C. Adachi, *Nature*, 2012, **492**, 234–238; (*e*) Q. T. Siddiqui, A. A. Awasthi, P. Bhui, M. Muneer, K. R. S. Chandrakumar, S. Bose and N. Agarwal, *J. Phys. Chem. C*, 2019, **123**, 1003–1014; (*f*) Y. Jiang, Y.-Y. Liu, X. Liu, H. Lin, K. Gao, W.-Y. Lai and W. Huang, *Chem. Soc. Rev.*, 2020, **49**, 5885; (*g*) Y. Jiang, M. Fang, S.-J. Chang, J.-J. Huang, S.-Q. Chu, S.-M. Hu, C.-F. Liu, W.-Y. Lai and W. Huang, *Chem. – Eur. J.*, 2017, **23**, 5448; (*h*) Y. Jiang, K. F. Li, K. Gao, H. Lin, H. L. Tam, Y.-Y. Liu, Y. Shu, K.-L. Wong, W.-Y. Lai, K. W. Cheah and W. Huang, *Angew. Chem., Int. Ed.*, 2021, **60**, 10007.

5 (*a*) J. N. Moorthy, P. Venkatakrishnan, D.-F. Huang and T. J. Chow, *Chem. Commun.*, 2008, 2146–2148; (*b*) C.-H. Chien, C.-K. Chen, F.-M. Hsu, C.-F. Shu, P.-T. Chou and C.-H. Lai, *Adv. Funct. Mater.*, 2009, **19**, 560; (*c*) I. Cho, S. H. Kim, J. H. Kim, S. Park and S. Y. Park, *J. Mater. Chem.*, 2012, **22**, 123.

6 (*a*) D. Chercka, S.-J. Yoo, M. Baumgarten, J.-J. Kim and K. Müllen, *J. Mater. Chem. C*, 2014, **2**, 9083–9086; (*b*) M.-Y. Lo, C. Zhen, M. Lauters, G. E. Jabbour and A. Sellinger, *J. Am. Chem. Soc.*, 2007, **129**, 5808–5809; (*c*) T. P. D. De Silva, S. G. Youm, G. G. Tamas, B. Yang, C.-H. Wang, F. R. Fronczek, G. Sahasrabudhe, S. Sterling, R. D. Quarels, P. K. Chhotaray, E. E. Nesterov and I. M. Warner, *ACS Omega*, 2019, **4**, 16867–16877; (*d*) C. Tang, F. Liu, Y.-J. Xia, J. Lin, L.-H. Xie, G.-Y. Zhong, Q.-L. Fan and W. Huang, *Org. Electron.*, 2006, **7**, 155–162; (*e*) M. Fang, J. Huang, Y. Zhang, X. Guo, X. Zhang, C.-F. Liu, W.-Y. Lai and W. Huang, *Mater. Chem. Front.*, 2017, **1**, 668.

7 (*a*) V. A. Montes, G. V. Zyryanov, E. Danilov, N. Agarwal, M. A. Palacios and P. Anzenbacher Jr, *J. Am. Chem. Soc.*, 2009, **131**, 1787–1795; (*b*) N. Agarwal, *Dyes Pigm.*, 2009, **83**, 328–333; (*c*) C.-F. Liu, T. Lu, W.-Y. Lai and W. Huang, *Chem. – Asian J.*, 2019, **14**, 3442–3448; (*d*) Y.-D. Jiu, C.-F. Liu, J.-Y. Wang, W.-Y. Lai, Y. Jiang, W.-D. Xu, X.-W. Zhang and W. Huang, *Polym. Chem.*, 2015, **6**, 8019.

8 (*a*) P. Stachelek, J. S. Ward, P. L. dos Santos, A. Danos, M. Colella, N. Haase, S. J. Raynes, A. S. Batsanov, M. R. Bryce and A. P. Monkman, *ACS Appl. Mater. Interfaces*, 2019, **11**, 27125–27133; (*b*) P. Pander, A. Swist, P. Zassowski, J. Soloducho and M. Lapkowski, *Electrochim. Acta*, 2017, **257**, 192–202; (*c*) N. Agarwal, P. K. Nayak, F. Ali, M. P. Patankar, K. L. Narasimhan and N. Periasamy, *Synth. Met.*, 2011, **161**, 466–473; (*d*) P. Pander, A. Swist, R. Motyka, J. Soloducho, F. B. Dias and P. Data, *J. Mater. Chem. C*, 2018, **6**, 5434–5443; (*e*) V. Joseph, K. R. J. Thomas, S. Sahoo, M. Singh and J.-H. Jou, *Dyes Pigm.*, 2018, **158**, 295–305.

9 (*a*) X. Liu, M. Sang, J. Zhou, S. Xu, J. Zhang, Y. Yan, H. Lin and W.-Y. Lai, *Mater. Chem. Front.*, 2020, **4**, 3660; (*b*) S.-K. Kim, B. Yang, Y. Ma, J.-H. Lee and J.-W. Park, *J. Mater. Chem.*, 2008, **18**, 3376–3384.

10 (*a*) J. Jayabharathi, S. Panimozhi and V. Thanikachalam, *Sci. Rep.*, 2019, **9**, 17555; (*b*) M. Idris, C. Coburn, T. Fleetham, J. Milam-Guerrero, P. I. Djurovich, S. R. Forrest and M. E. Thompson, *Mater. Horiz.*, 2019, **6**, 1179–1186; (*c*) D. Kathirvelan, S. Mayakrishnan, N. U. Maheswari, C. Biswas, S. S. K. Raavi and T. K. Panda, *New J. Chem.*, 2020, **44**, 1785–1794; (*d*) N. Agarwal, M. Patil and M. Patil, *RSC Adv.*, 2015, **5**, 98447–98455.

11 (*a*) Z. R. Grabowski, K. Rotkiewicz and W. Rettig, *Chem. Rev.*, 2003, **103**, 3899–4032; (*b*) A. Kapturkiewicz, J. Herbich and J. Nowacki, *J. Phys. Chem. A*, 1997, **101**(12), 2332–2344; (*c*) B. K. Sharma, A. M. Shaikh, N. Agarwal and R. M. Kamble, *RSC Adv.*, 2016, **6**, 17129–17137.

12 (*a*) J. Tagare, S. S. Swayamprabha, D. K. Dubey, R. A. Kumar Yadav, J.-H. Jou and S. Vaidyanathana, *Org. Electron.*, 2018, **62**, 419–428; (*b*) J. Tagare, D. K. Dubey, J.-H. Jou and S. Vaidyanathan, *ChemistrySelect*, 2019, **4**, 6458–6468.

13 M. R. D. Sylvinson, H.-F. Chen, L. M. Martin, P. J. G. Saris and M. E. Thompson, *ACS Appl. Mater. Interfaces*, 2019, **11**, 5276–5288.

14 (*a*) X. Cao, D. Zhang, S. Zhang, Y. Tao and W. Huanga, *J. Mater. Chem. C*, 2017, **5**, 7699–7714; (*b*) M. Chen, Y. Yuan, J. Zheng, We-C Chen, L.-J. Shi, Z.-L. Zhu, F. Lu, Q.-X. Tong, Q.-D. Yang, J. Ye, M.-Y. Chan and C.-S. Lee, *Adv. Opt. Mater.*, 2015, **3**, 1215–1219; (*c*) R. K. Konidena, K. R. Justin Thomas, D. K. Dubey, S. Sahoo and J.-H. Jou, *ChemPhotoChem*, 2020, **4**, 5364–5375; (*d*) Q. T. Siddiqui, P. Bhui, M. Muneer, K. R. S. Chandrakumar, S. Bose and N. Agarwal, *J. Phys. Chem. C*, 2018, **122**, 25804–25812; (*e*) N. B. Ukah, S. P. Senanayak, D. Adil, G. Knotts, J. Granstrom, K. S. Narayan and S. Guha, *J. Polym. Sci.*, 2013, **51**, 1533–1542; (*f*) U. Würfel, M. Seßler, M. Unmüssig, N. Hofmann, M. List, E. Mankel, T. Mayer, G. Reiter, J.-L. Bubendorff, L. Simon and M. Kohlstädt, *Adv. Energy Mater.*, 2016, **6**, 1600594.

15 (*a*) A. H. Cook and D. H. Jones, *J. Chem. Soc.*, 1941, 278–282; (*b*) A. Javid, M. M. Heravi, F. F. Bamoharram and M. Nikpour, *Ann. Chem.*, 1858, **107**, 199; (*c*) B. Radziszewski, *Ber. Dtsch. Chem. Ges.*, 1882, **15**, 1493; (*d*) A. I. Shienok, L. S. Koltsova, N. L. Zaichenko and V. S. Marevtsev, *Russ. Chem. Bull.*, 2002, **51**, 2050–2054; (*e*) B. Gu, L. Huang, N. Mi, P. Yin, Y. Zhang, X. Tu, X. Luo, S. Luo and S. Yao, *Analyst*, 2015, **140**, 2778–2784; (*f*) B. Wang, G. Mu, J. Tan, Z. Lei, J. Jin and L. Wang, *J. Mater. Chem. C*, 2015, **3**, 7709–7719; (*g*) M. Liu, X.-L. Li, D. C. Chen, Z. Xie, X. Cai, G. Xie, K. Liu, J. Tang, S.-J. Su and Y. Cao, *Adv. Funct. Mater.*, 2015, **25**, 5190–5198; (*h*) M. S. Subeesh, K. Shanmugasundaram, C. D. Sunesh, Y. S. Wonb and Y. Choe, *J. Mater. Chem. C*, 2015, **3**, 4683–4687.

16 (*a*) Y. Zhang, S. L. Lai, Q. X. Tong, M. F. Lo, T.-W. Ng, M. Y. Chan, Z. C. Wen, J. He, K. S. Jeff, X. L. Tang, W. M. Liu, C. C. Ko, P. F. Wang and C. S. Lee, *Chem. Mater.*, 2012, **24**, 61–70; (*b*) F. Zhang, W. Li, D. Wei, X. Wei, Z. Li, S. Zhang, S. Li, B. Wei, G. Cao and B. Zhai, *RSC Adv.*, 2016, **6**, 60264–60270; (*c*) A. O. Eseola, O. Adepitan, H. Goerls and W. Plass, *New J. Chem.*, 2012, **36**, 891–902; (*d*) H. Huang, Y. Wang, B. Wang, S. Zhuang, B. Pan, X. Yang, L. Wang and C. Yang, *J. Mater. Chem. C*, 2013, **1**, 5899–5908; (*e*) Y. Yuan, D. Li, X. Zhang, X. Zhao, Y. Liu, J. Zhang and Y. Wang, *New J. Chem.*, 2011, **35**, 1534–1540; (*f*) Z.-Y. Wang, J.-W. Zhao, P. Li, T. Feng, W.-J. Wang, S.-L. Tao and Q.-X. Tong, *New J. Chem.*, 2018, **42**, 8924–8932.

17 C. J. Kuo, T. Y. Li, C. C. Lien, C. H. Liu, F. I. Wu and M. J. Huang, *J. Mater. Chem.*, 2009, **19**, 1865–1871.

18 (*a*) Y. Zhang, S. L. Lai, Q. X. Tong, M. Y. Chan, T. W. Ng, Z. C. Wen, G. Q. Zhang, S. T. Lee, H. L. Kwong and C. S. Lee, *J. Mater. Chem.*, 2011, **21**, 8206–8214; (*b*) Y. Yuan, D. Li, X. Zhang, X. Zhao, Y. Liu, J. Zhang and Y. Wang, *New J. Chem.*, 2011, **35**, 1534–1540.

19 H. Hwang, C. Park, D. H. Sin, E. Song and K. Cho, *Org. Electron.*, 2020, **83**, 105738.

20 (*a*) I. R. Gould, R. H. Young, L. J. Mueller and S. Farid, *J. Am. Chem. Soc.*, 1994, **116**, 8176–8187; (*b*) H. Noda, H. Nakanotani and C. Adachi, *Sci. Adv.*, 2018, **4**, eaao6910, DOI: 10.1126/sciadv.aao6910; (*c*) J. Jayabharathi, P. Nethaji, V. Thanikachalam and R. Ramya, *ACS Omega*, 2019, **4**, 4553–4570; (*d*) Y. Zhang, S.-L. Lai, Q.-X. Tong, M.-Y. Chan, T.-W. Ng, Z.-C. Wen, G.-Q. Zhang, S.-T. Lee, H.-L. Kwong and C.-S. Lee, *J. Mater. Chem.*, 2011, **21**, 8206–8214.

21 (*a*) B. Valeur and M. N. Berberan-Santos, *Molecular Fluorescence: Principles and Applications*, Wiley-VCH, Weinheim, Germany, 2nd edn, 2012; (*b*) H. Huang, Y. Wang, S. Zhuang, X. Yang, L. Wang and C. Yang, *J. Phys. Chem. C*, 2012, **116**(36), 19458–19466; (*c*) Y. Zhang, J.-H. Wang, G. Han, F. Lu and Q.-X. Tong, *RSC Adv.*, 2016, **6**, 70800–70809.

22 G. Heinrich, S. Schoof and H. Gusten, *J. Photochem.*, 1974, **3**, 315–320.

23 (*a*) M. H. Tsai, H. W. Lin, H. C. Su, T.-H. Ke, C. C. Wu, F. C. Fang, Y. L. Liao, K. T. Wong and C. I. Wu, *Adv. Mater.*, 2006, **18**, 1216–1220; (*b*) W. Y. Hung, G. C. Fang, Y. C. Chang, T. Y. Kuo, P. T. Chou, S. W. Lin and K. T. Wong, *ACS Appl. Mater. Interfaces*, 2013, **5**, 6826–6831; (*c*) A. Michaleviciute, E. Gurskyte, D. Volyniuk, V. V. Cherpak, G. Sini, P. Y. Stakhira and J. V. Grazulevicius, *J. Phys. Chem. C*, 2012, **116**, 20769–20778.

24 (*a*) G. Gritzner and J. Kuta, *J. Pure Appl. Chem.*, 1984, **56**, 461–466; (*b*) P. K. Nayak, N. Agarwal, F. Ali, M. P. Patankar, K. L. Narasimhan and N. Periasamy, *J. Chem. Sci.*, 2010, **122**, 847–855.

25 F. Nesse, The ORCA program system, *Wiley Interdiscip. Rev.: Comput. Mol. Sci.*, 2012, **2**, 73–78.

26 (*a*) A. D. Becke, *J. Chem. Phys.*, 1993, **98**, 5648; (*b*) P. J. Stephens, F. J. Devlin, C. F. Chabalowski and M. J. Frisch, *J. Phys. Chem.*, 1994, **98**, 11623–11627.

